https://doi.org/10.1016/j.actamat.2019.03.007

Tunable tensile ductility of metallic glasses with partially rejuvenated amorphous structures

L. Zhao [a], K.C. Chan [a,*], S.H. Chen [b], S.D. Feng [a], D.X. Han [a], G. Wang [c]

[a] *Advanced Manufacturing Technology Research Centre, Department of Industrial and Systems Engineering, The Hong Kong Polytechnic University, Hung Hom, Kowloon, Hong Kong*

[b] *School of Mechanical Engineering, Hefei University of Technology, Hefei 230009, China*

[c] *Laboratory for Microstructures, Institute of Materials, Shanghai University, Shanghai 200444, China*

Submitted to

Acta Materialia

As a full paper

∗ Correspondence authors.

E-mail address: kc.chan@polyu.edu.hk (K.C. Chan)

Abstract

We report that the tensile ductility of metallic glass (MGs) is tunable by introducing gradient rejuvenated amorphous structures (GRASs) using large-scale atomistic simulations. The results reveal that the ductile GRASs promote the formation and propagation of new shear bands in the interior unrejuvenated region by suppressing the catastrophic propagation of individual shear bands across the GRASs, thus resulting in a more dispersed plastic shearing throughout the sample. It is also demonstrated that increasing both the volume fraction and degree of structural disordering of GRASs can improve the tensile ductility of MGs and lead to a brittle-to-ductile transition of the deformation mode, although at the expense of some strength. Moreover, the critical volume fraction of GRASs required for switching the transition is found to depend on the specific degree of structural disordering. The observed structural state-dependent transition of the deformation mode is further understood from a mechanical perspective by considering the competition between the macroscopic yield strength and the critical stress of the material required for shear delocalization, based on which a criterion is developed to predict the critical transition boundary in MGs with GRASs across a wide range of structural states. The findings provide a detailed atomistic understanding of the relationship between the structural state and mechanical properties in MGs with partially rejuvenated amorphous structures, which may offer useful insights for designing and processing MGs with a sought-after combination of ductility and strength.

Keywords: *Metallic glasses; Molecular dynamics; Gradient structure; Structural rejuvenation; Mechanical properties; Ductility*

1. Introduction

Metallic glasses (MGs) have aroused tremendous interest due to their exceptionally high elasticity and strength, high fracture toughness combined with attractive processing potential in the supercooled liquid region, all of which originate from the unique liquid-like atomic structure [1-3]. However, most MGs under tensile loading at ambient temperature suffer from a strong propensity towards shear localization into a few narrow regions, known as shear bands, which tend to propagate rapidly such that limited macroscopic plasticity is experienced before catastrophic failure [4, 5]. The severe brittleness of MGs severely deteriorates structural reliability, which is thus one major weakness that precludes their widespread applications as load-bearing materials [6, 7]. Consequently, considerable efforts have been dedicated to exploring the potential feasibility of ductilizing MGs. One effective approach is to enhance or introduce structural heterogeneities that may serve as effective obstacles to suppress the catastrophic propagation of individual shear bands at the early deformation stage, promoting the formation of multiple shear bands to deliver more plasticity and delay shear instability [8-10]. For instance, phase separation was verified to be beneficial for the ductility of some MGs by generating chemical inhomogeneities during quenching [11]. Besides, nanoglasses synthetized with hard cores and relative soft grain boundaries were observed with a brittle-to-ductile transition of the deformation mode when reducing the glass grain size [12-14]. In addition, MG-matrix composites [15, 16] and MG/crystalline metal nanolaminates [17] with considerable tensile plasticity were successfully fabricated by introducing ductile crystals, which serve as defects-like secondary phases for promoting the formation of multiple shear bands. Inspired by the concept of structural heterogeneities, for a given pure MG in bulk size, surface mechanical pre-treatments, such as surface mechanical attrition treatment [18] and shot penning [19], were also applied to induce

heterogeneous microstructures accompanied with beneficial compressive residual stress near the surface. The treated MGs were demonstrated to have improved ductility in subsequent bending and tensile tests.

Recently, it was found that exposure of MGs to ion bombardment can enhance spatially distributed structural heterogeneities without affecting the nature of the amorphous structure [20-26]. In this process of solid-state amorphization, since high temperature is not involved, the atomic structure could be rejuvenated to a highly disordered state. Meanwhile, the rejuvenation depth, i.e., the ion stopping range, is around 2 nm ~ 2 μm, with the specific value depending on the particle types (i.e., electron, protons or charged heavy ions) and the energy of the collision cascades, etc [23, 27]. Therefore, a moderate volume fraction of rejuvenated materials can be induced in nano- and microscale specimens. It was hypothesized that the structural heterogeneity induced by ion irradiation is characterized as a combination of severely rejuvenated surfaces and an intact interior regime [20, 21]. By irradiating $Zr_{52.5}Cu_{17.9}Ni_{14.6}Al_{10}Ti_5$ MGs in bulk size using 3 MeV Ni^+ ions, Perez-Bergquist et al. [21] found that Young's modulus and nanoindentation hardness both decreased by 20% from the centre to the surface, which indicates a gradient rejuvenated amorphous structure (GRAS) from the interior to the irradiated surfaces. A similar experimental study conducted by Bian et al. [23] also revealed an irradiation dosage-dependent softening, which is associated with the change of the glassy structures by increasing the free volume content. It has been argued that ion irradiation may act as an agent for structure rejuvenation, giving rise to reduced hardness and more disordered structures on irradiated surfaces, resulting in GRASs, which is reminiscent of the effect of exerting a much higher cooling rate near the surfaces than in the interior during quenching the liquid alloys [20].

Similar to the well-reported sensitivity of MGs subjected to different processing histories, irradiation-induced rejuvenation also has a significant influence on the mechanical properties of

micro- and nanoscale MGs after irradiation treatment. Raghavan et al. [28] examined structural softening in a series of heavily irradiated micropillars and found that the yield stress was reduced by 30%. Liu et al. [29] studied the effect of the focused ion beam (FIB), widely utilized for preparing micro- and nanoscale specimens, on the room-temperature deformation behaviour of Zr-based MG thin films under nanoindentation, and uncovered a reduction of the hardness and suppression of shear band formation in the FIB-milled MG films. Magagnosc et al. [20, 22] further reported a reversible transition of the deformation mode from brittle-like to ductile-like deformation in MG nanowires, which were originally prepared by the thermoplastic moulding method. They found that ion irradiation could induce tensile ductility, while subsequent annealing relaxed the nanowires to the initial brittle state. Furthermore, Tian et al. [30] demonstrated that even electron irradiation, commonly utilized for in-situ observations, could enhance the tensile ductility of nanoscale MGs at high current densities. So far, although some efforts have been undertaken to understand the influence of the structural state on the mechanical properties of MGs, no study has systematically investigated the structure-property relationships of MGs subjected to ion irradiation conditions. It is still challenging, experimentally, to quantitatively investigate the structure-property in real ion-irradiated MGs since precisely tailoring the spatial distribution of GRASs is difficult. Atomistic modelling, which allows one to probe the detailed deformation behaviour of materials as a function of the tailored architectures [31-33], is a powerful tool for probing this issue. Moreover, through atomic resolution visualization of the deformation process, one can establish links between the underlying atomistic mechanisms and the resultant properties of the materials [8, 34]. To the authors' best knowledge, so far, little attention has been given to systematically understand the structure-property relationship of MGs subjected to irradiation using molecular dynamics (MD) simulations.

In this work, we investigate the tensile deformation behaviour of irradiation-rejuvenated MGs through tailoring GRASs in the irradiated regions using large-scale atomistic simulations. By systematically varying the volume fraction and degree of structural disordering of GRASs, a brittle-to-ductile transition of the deformation mode was observed in certain combinations of the volume fraction and degree of structural disordering. To gain a more direct and quantitative insight into the structure-property relationship in the partially rejuvenated MGs with GRASs, the critical boundary required for switching the transition was identified by introducing a critical stress criterion for shear delocalization. Moreover, both the sample size and aspect ratio of the MGs were found to affect the brittle-to-ductile transition.

2. Simulation Methods

Large-scale atomistic simulations were implemented using LAMMPS [35]. The $Cu_{64}Zr_{36}$ (at.%) binary MG was chosen for its ease of atomistic modelling and extensively studied atomic structure [36, 37]. The embedded-atom-method potential developed by Sheng et al. [38] was adopted to describe the interactions between atoms. The time step for numerical integration was chosen to be 2 fs for all simulations. To construct the monolithic MG (thereafter denoted as "M-MG"), the "melt-quench-duplicate-anneal" procedure was implemented, following the description in the literature [33]. Briefly, a random $Cu_{64}Zr_{36}$ configuration, containing 30000 atoms, was homogenized at 2000 K and zero external pressure for 2 ns with periodic boundary conditions (PBCs) imposed in all three dimensions. Then, the molten alloy was quenched at a cooling rate of 10^{10} K/s to the glassy state (100 K), which was further duplicated to the final dimension of the M-MG, followed by annealing at 800 K (the glass transition temperature, $T_g \approx 787$ K) for 0.5 ns, and finally brought back to 100 K. The prepared M-MG, of dimensions approximate 50 (X) ×4.8 (Y) ×100 (Z) nm^3, corresponds to a total atomic number of 1.5 million.

The MG samples partially rejuvenated with GRASs (hereafter labelled as "G-MGs") were constructed using the M-MG as the precursor according to the schematic diagram displayed in **Fig. 1**. In comparison with the M-MG, the hypothetical G-MGs were comprised of three subdivisions, i.e., two "irradiation-rejuvenated" regions with GRASs near the surfaces and an intact region in the centre. For simplicity, G-MGs adopted in this study were set to be symmetric along the X-direction. Given that the width of the sample is W and the depth of GRAS is L, the total volume fraction of the GRAS is then $2L/W \times 100\%$. Meanwhile, considering that the rejuvenated regions suffer from different levels of irradiation damage from the surfaces to the interior of the samples [23, 26], these regions were further subdivided into three layers, i.e., the surface layer, the middle layer and the inner layer (thereafter labelled as layers A, B and C, respectively), all of which have the same thickness ($3/L$) but with different levels of structural rejuvenation. To fabricate G-MGs with such GRASs, a "replaced-relax" procedure was implemented. Initially, small percentages of Zr atoms (8%, 6% and 4% for the A, B and C layers, respectively) were randomly selected and replaced with Cu atoms in the three layers. Then, 4.5%, 3.375% and 2.25% of Cu atoms were also randomly chosen and set as Zr atoms in the corresponding layers. It is noted that the Zr and Cu atoms in each layer were individually exchanged in such a way that the total proportions of the exchanged atoms increased from the interior to the surface, while the compositions in each layer were still unchanged. After that, the modified sample was kept at 100 K under zero external pressure for up for 0.5 ns to fully relax the atomic configuration. The boundaries in the X-direction were set as non-PBCs to imitate free surfaces during this process. Due to the large difference (~23.4%) in atomic radius between the Zr (1.58 Å) and Cu (1.28 Å) atoms, such artificial rearrangements of the local atomic configurations would induce high access energy and structural disturbances, which could be expected to induce structural modifications. To fabricate G-MGs

with GRASs across a wide range of structural states, the above "replace-relax" procedure was performed for several times. For simplicity, the corresponding structural states of GRASs in the obtained G-MGs were thereafter denoted as E*n*, where *n* is the time of atomic rearrangements. Meanwhile, the corresponding volume percentages of GRASs were labelled as P*m*, where *m* is the volume fraction of GRASs. Note that, in the case of the same sample size, a G-MG fabricated through the above-mentioned atomic rearrangements can be retrieved by a combination of these two parameters. For instance, the abbreviation for the "P50 E2-state G-MG" refers to a rejuvenated sample containing the E2-state GRAS, of which the total volume fraction is 50%.

The samples were subsequently elongated along the Z-direction at 100 K via iteratively rescaling the corresponding cell at an equivalent strain rate of 1×10^{8} s^{-1}. The non-PBC condition was present along the X-direction to allow for the occurrence of shear offset. The deformation was monitored using the atomic shear strain, η^{Mises}, calculated by comparing the atomic configurations between the deformed state and the state prior to loading [39]. Generally, the regions mapped with $\eta^{Mises} > 0.2$ represent clusters of local atoms undergoing collectively inelastic shearing in response to external force, and can be regarded as volumes of materials involved in shear transformation zones (STZs) [40]. To evaluate the fractions of atoms participating in plastic deformation, the "deformation participation ratio" parameter [33], $\psi = N^{\eta>0.2}/N$, was employed, where N and $N^{\eta>0.2}$ represent the total atoms in the sample and the number of atoms involved in STZs, respectively. Furthermore, to measure the deformation inhomogeneity, the "degree of shear localization" parameter [41], $\delta=\sqrt{\sum_{i=1}^{N}(\eta_i-\bar{\eta})^2/N}$, was introduced, where η_i is the local atomic shear strain of *i*-atom, and $\bar{\eta}$ is the averaged atomic shear strain of the entire sample. The visualization was implemented using OVITO [42].

3. Results

3.1. Structural characterization of GRASs

As an illustration, a series of P60 G-MGs fabricated with different times of atomic rearrangements (thus, different irradiation degrees) are used to characterize the structural evolution. The GRASs in the rejuvenated regions are examined by calculating the radial distribution functions (RDFs) [43]. As shown in **Fig. 2**, the RDF patterns are characteristic of fully amorphous structures, implying that no crystallization occurs during the process of emulated irradiations. However, subtle changes around the second-nearest neighbour shell (marked by the red box) are detectable, as manifested in the **inset of Fig. 2**. It can be seen that, with increasing the times of atomic rearrangements, the position of the second peak slightly shifts toward a higher *r*-value, and the succedent peak splitting, as observed in the original E0-state sample (i.e., the M-MG), gradually disappears. These variations are reminiscent of structural rejuvenation of amorphous materials, which point to a more liquid-like state [44, 45].

To further reveal the underlying structural modifications, the atomic-scale topological structures were analyzed in terms of topological short-range orders (SROs) employing the weighted-Voronoi tessellation [46]. So far, the atomic structures and mechanical properties of the $Cu_{64}Zr_{36}$ M-MG have been extensively studied, with a consensus that the dominating structural motif of topological SROs is the Cu-centred full icosahedral (FI), i.e., Voronoi polyhedrons with index [0,0,12,0], which exhibits a relatively high packing density, stable configurational state and shear resistance [46, 47]. These FI clusters are spatially interconnected and assumed to constitute the structural skeleton that is responsible for the strong-but-brittle behaviour of the MG [47, 48]. Consequently, the fraction of Cu-centred FI clusters with respect to the total number of Cu atoms was adopted as a structural indicator to characterize the SROs behind the amorphous structures.

Fig. 3(a) shows the evolution of the Cu-centred FI frictions in the P60 G-MG series, along with the M-MG for comparison. In addition, **Fig. 3(b)** and **Fig. 3(c)** demonstrate the variations of the local average Voronoi volumes of the Zr and Cu atoms, based on which one can evaluate the relative changes of the free volume [49]. It is clear to see significant changes in the rejuvenated regions with GRASs (i.e., the zones highlighted in grey). The Cu-centred FI frictions decrease gradually from the interior to the free surfaces, albeit with some fluctuations, revealing an analogous radiant fluence-dependent disordering process, as reported in previous experiments [20, 23, 50], and MD simulations [24, 26]. Concomitantly, both the local average Voronoi volumes of the Zr and Cu atoms increase with increasing the times of atomic arrangements, as shown in **Fig. 3(b)** and **Fig. 3(c)**, a manifestation of a net generation of the free volume from the interior to the free surfaces [49]. Clearly, the GRASs in these G-MGs display a feature of gradient rejuvenated structures with higher degrees of structural disordering and more free volume near the surfaces, as compared with the case of the M-MG. It is also worth noting that the structural changes become less distinct after more than five times of atomic arrangements. This indicates that the degree of structural disordering approaches saturation afterwards, even though the amorphous matrix is more heavily manipulated. In the literature, Mayr [25] reproduced the process of collision cascades occurred in ion irradiation using atomistic simulation and found that ion irradiation could destroy icosahedral clusters and increase the free volume, giving rise to the successive rejuvenation of amorphous structures toward a steady state, which is independent of the initial state. Another similar study conducted by Avchaciov et al. [26] also supported the above standpoint through analysing the chemical and topological SROs. Therefore, we believe that the structural disturbances, activated by the artificial atomic rearrangements adopted in this study, destroy topological SROs and induce structural rejuvenation, playing a role analogous to collision cascades

induced by exotic energetic particles. From the above analysis, one can recognize that the GRASs obtained in the irradiated regions are endowed with looser packing atomic structures and more free volume contents, as compared to the atomic configuration in the inner unrejuvenated region. The GRASs promote glassy heterogeneities within the samples and may lead to customizable mechanical properties of the G-MGs under mechanical loading [8].

Before the mechanical tests, it is noteworthy that the above structural rejuvenation process of GRASs has a negligible influence on the internal stress distributions in the G-MGs. For clarification, **Fig. 3(d)** depicts the distributions of the local stress along the Z-direction (σ_z) in the P60 G-MGs. The profiles of σ_z in the five G-MGs almost coincide with that of the M-MG, albeit with some fluctuations. Although all the samples suffer from a high level of tensile stresses on the surfaces due to the high surface free energy [51], their amplitudes are comparable with each other, and the affected thicknesses are limited to within 0.5 nm on the free surfaces. They are expected to have no impact on the deformation behaviour of G-MGs in this study because previous atomistic studies associated with the sample size effects on the mechanical behaviour of MG nanowires revealed that the influence of the surface tensile stress could be ignored when the sample size exceeds 20 nm [51, 52]. Therefore, these "residual stress-free" G-MGs prepared in this study can serve as ideal models to directly evaluate the change of structural states, i.e., the existence of GRASs, on the tensile deformation behaviour of G-MGs.

3.2 The effect of volume fraction of GRASs on the tensile deformation behaviour

Firstly, we examine the effect of volume fraction of GRASs on the tensile deformation behaviour of the G-MGs. Ten G-MGs were fabricated with varied GRASs having the same degree of structural disordering (the E4 state) but different volume fractions ranging from 10 to 100%, with intervals of 10%. It should be noted that the E4 state of the GRAS was chosen here due to the

relatively high level of structural rejuvenation as displayed in **Fig. 3**, which is more favourable for shear delocalization under deformation.

The representative tensile stress-strain (SS) curves of the series of the E4-state G-MGs are depicted in **Fig. 4(a)**, together with that of the M-MG (i.e., the P0 sample) for comparison. Concomitantly, the evolutions of the peak stress (σ_p) and Young's modulus (E) with the volume fraction are presented in the **inset of Fig. 4(a)**. In line with previous studies [37, 53], σ_p is regarded as the critical stress needed to induce macroscopic plastic flow, i.e., corresponding to the macroscopic yield strength. E is derived from the initial linear SS relationships with the applied strain $\varepsilon < 2.5\%$ in the SS curves. It is observed that the macroscopic yield points (ε_p) for the G-MGs are nearly the same, which suggests that ε_p is independent of the structural states in the G-MGs. However, both the σ_p and E values decrease gradually with increasing the volume fraction from 0 to 100%. This clearly indicates a softening trend of the G-MGs by introducing GRASs. In addition, the evolution of σ_p and E as a function of volume fraction approach nearly linear relationships, as shown in the **inset of Fig. 4(a)**, following the rule-of-mixtures prediction. The observation of reduced σ_p and E in G-MGs is consistent with those found in tensile experiments on ion-irradiated MG nanowires [20, 22, 23]. One can also observe, from the SS curves, that the M-MG demonstrates a typical abrupt stress drop immediately upon exceeding the peak, which is attributed to the rapid spontaneous localization of severe plastic shearing into one dominating shear band and is regarded as a characteristic of poor ductility in M-MGs [54]. In contrast, for the G-MGs that are partially rejuvenated with GRASs, the rate of stress drop tends to be lower and, more importantly, reduces gradually with increasing volume fraction. Moreover, the overall flow stress at the post-yielding stage (i.e., $\varepsilon > 10\%$) augments inversely. When the volume fraction exceeds 50%, the flow stress reaches a plateau and maintains the same stress level even at $\varepsilon > 24\%$,

which indicates an apparent feature of ductile deformation behaviour [40]. The SS curves unambiguously reveal that there exists a brittle-to-ductile transition of the deformation mode at a critical volume fraction of the GRASs around 50% in the E4-state G-MGs.

Fig. 4(b) shows the evolution of ψ (see **Simulation Methods**) as a function of ε in the G-MGs, together with δ (see **Simulation Methods**) as a function of the volume fraction of GRASs at ε = 24% in its **inset**. Note that a larger ψ suggests a higher volume proportion of material involved in plastic deformation, while a larger δ implies a higher propensity of shear localization via shear banding [8, 55]. More specifically, for samples undergoing superplastic deformation, $\psi \approx 1$ while $\delta \approx 0$. In all, ψ increases monotonously with increasing ε in each sample, and also augments with increasing the volume fraction of GRASs at any given ε. An intriguing observation here is that, with increasing the volume fraction of GRASs in the G-MGs, ψ increases in a manner more proportional to ε, which implies that more atoms cumulatively participate in the process of plastic deformation [33]. In the post-yielding stage ($\varepsilon > 10\%$), a striking increase of ψ is observed as the volume fraction reaches 50%, which is correlated with the transition of the deformation mode as revealed in the SS curves. Furthermore, the evolution of δ as a function of the volume fraction at ε = 24%, as shown in the **inset of Fig. 4(b)**, demonstrates that δ first decreases with increasing the volume fraction and then reaches a plateau, with the value approaches zero as the volume fraction exceeds 50%, further supporting the existence of the brittle-to-ductile transition in the E4-state G-MGs.

To further uncover the above-mentioned transition, **Fig. 5(a)-(c)** display a sequence of deformation patterns under different applied strains in the E4-state G-MGs around the critical volume fraction, i.e., the P40, P50 and P60 G-MGs, respectively. The first rows display the initial plastic deformation at ε = 6.0% in the samples. It is seen that the initial plasticity was triggered

by activation of multiple scattered STZs in the GRASs due to their relatively soft structures. With further loading, these STZs tend to proliferate discretely to higher density, rather than aggregate and grow in a cooperative manner and serve as nuclei of shear bands near the free surfaces, as generally observed in the uniaxial deformation process of M-MGs [46, 56]. Correspondingly, the hard unrejuvenated region deforms almost elastically under the iso-strain condition. Upon reaching a critical ε of 7.7%, plastic deformation occurs in the unrejuvenated region through the nucleation of embryonic shear bands (marked by the ellipses at ε = 7.7% in **Fig. 5**). It is noted that the propagation of these early generated embryonic shear bands tends to be impeded upon encountering the boundaries of GRASs soon after their formation (see ε = 9.2% in **Fig. 5**). With further deformation, more embryonic shear bands are involved in plastic deformation in the hard unrejuvenated region to accommodate the plastic flow in the soft GRASs (see ε = 14.0% in **Fig. 5(b)-(c)**). It appears that the ductile GRASs act as heterogeneous barriers, which suppress the catastrophic propagation of individual shear bands across the GRASs at the early deformation stage, promoting the formation and propagation of new embryonic shear bands in the hard unrejuvenated region. The impeding effect of the GRASs to the unstable shear band propagation should be more pronounced with increasing the volume fraction of the GRASs from 40% to 60%. Thus, the number of accumulated shear bands in the hard unrejuvenated region augments from the P40 G-MG to P60 G-MG (see ε =14.0% in **Fig. 5**). Generally, a higher density of shear bands would promote a more distributed plastic deformation throughout the sample and may contribute to a transition of the deformation and failure mode at large ε [40, 57]. It is seen that, in the P40 G-MG, only two shear bands are generated due to the limited impeding effect of the GRAS to the shear band propagation. These two shear bands successfully penetrate the entire sample with the below one producing the main shear offset on the surfaces, an indication of highly localized

deformation behaviour via shear banding (see **Fig. 5(a)** and **Supplementary Video S1**). While, the P50 G-MG exhibits necking behaviour, a relatively ductile mode of tensile deformation due to the interactions of a high density of embryonic shear bands generated near the middle of the length of the sample (see **Fig. 5(b)** and **Supplementary Video S2**). More strikingly, for the P60 G-MG, a high density of embryonic shear bands and STZs generated along the length direction in the unrejuvenated region greatly promotes the redistribution of plasticity, which finally results in homogeneous-like plastic flow (see **Fig. 5(c)** and **Supplementary Video S3**). The direct observation of the transition from the deformation patterns as the volume fraction of GRASs reaches the critical value of 50% is consistent with the foregoing results from the SS curves, as displayed in **Fig. 4(a)**.

3.3 The effect of degree of structural disordering of GRASs on the tensile deformation behaviour

With the volume fraction effect of GRASs on the transition of deformation mode established, we further turn our focus to examine the effect of the degree of structural disordering of GRASs. To this end, we constructed four G-MGs (hereafter denoted as E1, E2, E3 and E4-state samples), which were prepared under different times of atomic rearrangements but with a constant volume fraction of GRASs of 60%. The thickness of the GRASs was fixed to be 15 nm. The detailed structural evolutions of GRASs in these G-MGs are presented in **Fig. 2**.

Fig. 6(a) displays the tensile SS curves for the P60 G-MGs along with the M-MG (i.e., the E0-state sample), for comparison. It is observed that σ_p and E decrease with increasing the degree of structural disordering of GRASs from the E0 to the E4 state. The evolution of σ_p and E is plotted in the **inset of Fig. 6(a)**. Evidently, both σ_p and E are inclined to level off at high degrees of structural disordering, which is consistent with the gradually saturated tendency of structural rejuvenation revealed in **Fig. 3**. One can also observe that, after global yielding, the amplitude of

the stress drop declines progressively, an indication of improved tensile ductility. This suggests that the tensile ductility of G-MGs can be also improved by tuning the degree of structural disordering of GRASs, even though their volume fractions are identical. At large applied strains, i.e., $\varepsilon = 20\%$, there is a significant increase of the flow stress as the degree of structural disordering of GRASs increases from the E0 to E1 state and from the E1 to E2 state, while the corresponding changes from the E2 to E3 state and from the E3 to E4 state are much smaller. The contrast is also demonstrated in **Fig. 6(b)**, in which the evolution of ψ is plotted as a function of ε in the P60 G-MGs. It is clear to see a striking increase of ψ at the post-yielding stage ($\varepsilon > 10\%$) as the degree of structural disordering crosses the E1 and E3 states. Meanwhile, the change of δ at $\varepsilon = 24\%$ as a function of the degree of structural disordering (**inset of Fig. 6(b))** demonstrates that δ tends to reach a plateau which approaches zero when the degree of structural disordering exceeds the E2 state. These results all clearly imply a significant change of the deformation mode in the series of the P60 G-MGs around the critical degree of structural disordering of the E2 state.

The final deformation patterns of the series of the P60 G-MGs at $\varepsilon = 24\%$ are demonstrated in **Fig. 6(c)**. For better visualization, atoms in the operating STZs (i.e., atoms with $\eta^{Mises} > 0.2$) within the GRASs are coloured according to their specific values of η^{Mises}, while the others are coloured in cyan. As expected, an intriguing transition of the deformation mode from highly localized shear banding to ductile necking and then homogeneous-like plastic deformation is observed with increasing the degree of structural disordering of GRASs from the E0 to E4 state. Consistent with the foregoing observations in the E4-state G-MGs shown in **Fig. 5**, embryonic shear bands are also generated in the interior unrejuvenated region of all the P60 G-MGs, although the GRASs suffer from different disordering degrees (see **Supplementary Fig. S1**). A close observation of the deformation patterns found that the density of STZs in the GRASs augments

progressively with increasing the degree of structural disordering of GRASs from the E1 to E4 state. In this regard, one can speculate that the impeding effect of GRASs that suppresses the unstable shear band propagation across GRASs tends to be strengthened. For the E1-state G-MG, the GRASs cannot effectively impede the dominating shear band extended from the interior unrejuvenated region due to the lowest degree of structural disordering. Therefore, the E1-state G-MG deforms in a manner similar to the M-MG, i.e., via one dominating shear band that penetrates the entire sample (see **Supplementary Video S4**). In contrast, more shear bands are successfully induced in the interior unrejuvenated regions with increasing the degree of structural disordering of GRASs. At large ε, these shear bands in the unrejuvenated regions and the fertile STZs in the GRASs deform cooperatively, leading to the redistribution of plasticity and bringing more materials into plastic deformation. As a result, the deformation mechanism of the P60 G-MG gradually evolves into ductile necking in the E2 state (see **Supplementary Video S5**) and further into homogeneous-like plastic deformation in the E3 (see **Supplementary Video S6**) and the E4 state (see **Supplementary Video S3**).

4. Discussion

Up to now, we have shown a brittle-to-ductile transition by systematically tailoring the volume fraction and degree of structural disordering of GRASs in the G-MGs. By excluding the effect of residual stress in the samples, the observed transition is regarded as a direct consequence of changing the structural state behind the random-like configurations. It is demonstrated that increasing both the volume fraction and degree of structural disordering of GRASs can improve the tensile ductility of G-MGs, which may result in the transition of deformation mode, although at the expense of some strength. Nevertheless, the critical volume fraction of GRASs required for switching the transition depends on its specific degree of structural disordering. It should be noted

that such GRASs-induced transition of the deformation mode has also been observed in recent experimental investigations on the uniaxial deformation behaviour of ion-irradiated nanosized MGs [20, 22, 23, 28], although the underlying deformation mechanism is still elusive. In this section, our attention is further focused on the atomistic mechanism of the GRASs-induced transition of deformation mode in the G-MGs and exploring a criterion to predict the transition across a wide range of structural states.

4.1. Size effect

The G-MGs were segmented into three subdivisions along the width direction with varied individual layer thickness, which reminds us of the possibility of size effect on the observed transition of deformation mode. Actually, improved plasticity or even shifted deformation mode can be achieved in MGs and MG composites by decreasing the sample size or the characteristic sizes of the dominating phases to the nanometre range, as corroborated by extensive experimental and computational investigations [58-61]. For instance, using *in situ* tensile tests, Jang and Greer [58] and Guo et al. [59] observed a brittle-to-ductile transition and a metal-like ductility in Zr-based MG nanopillars when reducing the dimensions of specimens to 100 nm and below. While the critical size detected through atomistic simulations is generally much smaller, probably due to the applied superfast strain rate (generally at the level of 10^8 s^{-1}) limited by the approach [62, 63]. Zhong et al. [63, 64] investigated the sample thickness-dependent tensile deformation behaviour of CuZr binary MGs using atomistic simulations and detected that the critical thickness for the transition ranged from 2.98 nm to 6.78 nm, depending on the chemical compositions. Other simulations also support the size-independent shear banding behaviour of MGs until the sample sizes approach the thickness of shear bands, i.e., 4 nm ~ 10 nm [65, 66]. It is noted that, in this atomistic study, the critical transition from brittle to ductile deformation was observed in the P50

E4-state G-MG and the P60 E2-state G-MG, as shown in **Fig. 5** and **Fig. 6**, respectively. The layer thicknesses of the rejuvenated regions and the interior intact region for the two samples correspond to 10 nm and 30 nm, 12.5 nm and 25 nm, respectively, all of which are higher than these foregoing thickness thresholds for the brittle-to-ductile transition in M-MGs. Therefore, the size effect is inadequate to rationalize the observed transition in G-MGs.

It should be noted, however, that sample size influences the critical boundary required for switching the transition in G-MGs. The sample widths of the above investigated samples were all fixed to 50 nm. As revealed in **Fig. 5(b)**, the brittle-to-ductile transition takes places as the volume fraction of GRASs reaches 50% in the E4-state G-MGs with the sample width of 50 nm. However, as the sample width is reduced to 30 nm, the critical volume fraction required for switching the transition decreases to 40%, as shown in **Fig. S2 (**see **Supplementary Fig. S2)**. It is evident that reducing the sample size promotes the brittle-to-ductile transition in G-MGs.

4.2. Mechanisms for the brittle-to-ductile transition

As illuminated above, embryonic shear bands tend to nucleate in the interior of the unrejuvenated region, carrying the main plastic deformation of this region upon its yielding. At the moment of the shear band nucleation (i.e., ε = 7.7% in **Fig. 5**), obvious plastic deformation already occurs in the GRASs via homogenously distributed STZs. Moreover, the critical strain for the shear band nucleation in the unrejuvenated regions of all the G-MGs is very close to that of the M-MG (ε = 7.73%, as observed in **Fig. 7** in the later section). From these perspectives, the ductile GRASs seems not to directly act as heterogeneous sources for the formation of multiple shear bands in the unrejuvenated regions under the iso-strain deformation condition. Instead, they serve as effective barriers, suppressing the catastrophic propagation of individual shear bands generated in the unrejuvenated regions across the GRASs, delaying shear instability. It should be noted that

the same effect of the soft phase in a two-phase (hard and soft) amorphous structure was observed in a recent work conducted by Scudino et al. [67]. With further deformation, in the unrejuvenated regions more embryonic shear bands are generated and participate in plastic deformation to accommodate the plastic flow in the ductile GRASs. It is clear that the interactions between the ductile GRASs and the shear bands generated in the unrejuvenated regions contribute to the observed ductility enhancement in the G-MGs. Generally, increasing both the volume fraction and degree of structural disordering of GRASs can promote the impeding effect of GRASs to the shear band propagation, rendering more stable plastic deformation in the unrejuvenated regions. Therefore, increasing both the two structure parameters of GRASs can effectively improve the tensile ductility of G-MGs.

It should be emphasized that the ductilizing mechanisms of G-MGs with GRASs are essentially different from those found in extensively investigated amorphous/crystalline metal nanolaminates, in which crystalline metals, such as Cu, were introduced as the ductile heterogeneities [17, 33, 68]. By compressing $Cu_{46}Zr_{54}$/Cu(111) nanolaminates under the iso-strain condition, Arman et al. [68] found that the Cu layers act as heterogeneous sites for triggering multiple shear bands in the glassy layers through the transfer of dislocation plasticity from the Cu layers. With the consideration of grain boundaries in the Cu layers, Cheng and Trelewicz [69] further observed that the Cu layers yield much earlier than the glassy layers through the emission of lattice dislocations. They also concluded that the lattice dislocations induce stress concentrations when impinging on the amorphous-crystalline interfaces, which can effectively promote shear transformations of atoms in the glassy layers. Other previous studies [17, 31] on CuZr/crystalline metal nanolaminates under the iso-strain tensile condition also supports the above viewpoint. However, in this atomistic study, we found that the early embryonic shear bands generate

intrinsically in the unrejuvenated regions of G-MGs. The heterogenous GRASs do not actively promote the formation of multiple shear bands in the unrejuvenated regions through the transfer of the plasticity from the GRASs. This may due to the homogeneously distributed plastic deformation of the GRASs through a non-dislocation based mode, i.e., via scattered STZs, which is insufficient to induce substantial stress concentration at the interfaces between the heterogeneous regions [40].

It is worth noting, however, that the observed ductilizing mechanisms in G-MGs are in accordance with several previous atomistic studies that are associated with the tensile ductility improvement of MG/nanoglass nanolaminates [40] and nanoglass/MG/nanoglass sandwich structures [70] through incorporating ductile nanoglasses in MGs. As revealed in the pioneering work conducted by Şopu et al. [14, 55], the nanoglasses themselves contain a large population of soft glass-glass interfaces, i.e., glassy grain boundaries, having more rejuvenated structural states than the MG precursor. When reducing the glassy grain size to a critical value, the abundant soft interfaces can effectively promote shear delocalization and lead to homogeneous plastic flow in the nanoglasses [12, 71]. In the reported MG/nanoglass nanolaminates [40] and nanoglass/MG/nanoglass sandwich structures [70], the introduced ductile nanoglass layers were also found to impede the propagation of shear bands that spontaneously generated in the MG layers, playing a crucial role similar to the GRASs in G-MGs. We also note that, although the tensile ductility was improved in the nanoglass/MG/nanoglass sandwich structure [70], necking or homogenous-like deformation patterns did not appear. This may be ascribed to the low volume fraction (40%) and the low overall degree of structural disordering (considering that only the glass-glass interfaces were rejuvenated) of the nanoglass layers.

4.3. The critical stress for the brittle-to-ductile transition

To gain a more direct and quantitative insight into the structural state-dependent transition of the deformation mode in G-MGs, we further consider the critical condition required for switching the transition from a mechanical perspective. It is accepted that a critical stress (σ_{cr}) is needed for activating the aggregation of STZs into the formation of shear bands [8, 39, 46, 72]. Furthermore, σ_{cr} can be regarded as the intrinsic resistance of the MG to the propagation of a mature shear band. If σ_{cr} cannot be achieved in the MG under successive deformations, the propagation of the incipiently generated embryonic shear band would stagnate immediately upon its formation. In turn, more embryonic shear bands would be generated to accommodate local plastic deformation, thus giving rise to a tendency of strain delocalization from the highly localized shear bands [8, 39, 73]. In other words, the occurrence of strain delocalization is directly associated with the competition between the macroscopic yield strength (σ_p) of the material and the critical stress (σ_c) required for forming a mature shear band. One should note that the formation of a mature shear band is a short transient process, which occurs instantly once σ_{cr} is achieved [39, 46]. To ascertain the value of σ_{cr}, it is necessary to identify the critical moments when the shear band starts to initiate and propagate in the M-MG. In this study, by reducing the inspection interval of the deformation process during the tensile simulation, the two corresponding critical states are captured and displayed in **Fig. 7(a)** and **Fig. 7(b)**, respectively. At $\varepsilon = 7.73\%$, the shear localization commences by aggregating small STZs near the left free surface, resulting in the initiation of an embryonic shear band. With further increasing ε up to 8.28%, the embryonic shear band grows into a mature one which extends exactly to the right surface, penetrating the entire sample. The SS curve of the M-MG shown in **Fig. 4(a)** predicts two stress values around 2.89 GPa and 2.34 GPa for these two corresponding moments. Hence, σ_{cr} for the formation of a mature shear band is

identified to be within a range of 2.34 GPa and 2.89 GPa. It is important to note that the lower limit of σ_{cr} (2.34 GPa) required for highly localized shear banding can be taken as the upper limit of σ_{cr} required for strain delocalization. As a sequence, the critical stress for predicting the transition from the mechanical perspective can be expressed as follows: ductile behaviour via necking or homogenous-like flow if the macroscopic yielding stress $\sigma_p < \sigma_{cr}$ (σ_{cr}= 2.34 GPa), otherwise brittle behaviour via highly localized shear banding. Using the same criterion, Zhou et al. [8] successfully explained the atomic percent-dependent and orientation-dependent plastic transition behaviour in MGs embedded with the pre-existing shear bands, verifying the reliability of this criterion.

The above criterion provides us with a simple way to rationalize the observed transition of the deformation mode in the simulated G-MGs. In the series of the E4-state G-MGs rejuvenated with varied volume fractions of GRASs, σ_p is not reduced below σ_{cr} until the volume fraction of GRASs reaches 50% (**see Supplementary Fig. S4(a)**). Similarly, in the series of the P60 G-MGs with different degrees of structural disordering of GRASs, σ_p is larger than σ_{cr} until the degree of structural disordering of GRASs reaches the E2 state (**see Supplementary Fig. S4(b)**). According to the criterion, for these samples with $\sigma_p > \sigma_{cr}$ (i.e., the P0 ~ P40 E4-state G-MGs, and the E0 and E1-state P60 G-MGs), the resultant σ_p is sufficient to overcome the intrinsic resistance for the propagation of a mature shear band. Therefore, the deformation and failure patterns of these G-MGs are featured by individual highly localized shear band(s), as displayed in **Fig. 5** and **Fig. 6**. While, for the rest of the samples with higher volume fractions and higher degrees of structural disordering of GRASs in these two groups of G-MGs, since $\sigma_p < \sigma_{cr}$, highly localized shear banding tends to be suppressed. Instead, ductile necking behaviour and even homogeneous-like plastic flow

may be obtained. It is obvious that the critical transition points predicted from the criterion are in good conformity with the simulated results.

4.4. The deformation map for the brittle-to-ductile transition

Further effort was put on identifying the critical boundary of structure states required for switching the brittle-to-ductile transition in G-MGs across a wide range of structural states. For this purpose, the rule of mixtures under iso-strain conditions [74] was introduced to construct a mathematical model to predict the evolution of σ_p in G-MGs. In this study, σ_p was successfully parameterized with the volume fraction and degree of structural disordering of GRASs in G-MGs, which can be expressed as

$$\sigma_p = \sigma_{M\text{-}MG} \times (100\text{-}m)/100 + \sigma_p(n) \times m/100 \quad \text{GPa}$$

where m is the volume fraction of the GRAS in the G-MG, and n is the required times of atomic rearrangements for generating the same degree of structural disordering of the GRAS in the corresponding P100 G-MG. $\sigma_{M\text{-}MG}$ is the macroscopic yield strength (3.07 GPa) for the M-MG. $\sigma_p(n)$ describes the evolution of the macroscopic yield strength for the P100 G-MGs as a function of the times of atomic rearrangements, and was determined as $\sigma_p(n) = 1.45 + 1.62 \times \exp(-0.911 \times n)$ GPa. More detailed information about the fitting process as well as the verification is provided in the **Supplementary Materials**. **Fig. 8** demonstrates the evolution of σ_p in G-MGs with GRASs across a wide range of structural states, as predicted by the parameterized σ_p.

We further compare the parameterized σ_p with σ_{cr}, i.e., solving the inequation $\sigma_p < \sigma_{cr}$, so that the influence of the volume fraction and degree of structural disordering of GRASs on the transition can be systematically evaluated. This leads to a deformation map as displayed in **Fig. 9**, based on which the regimes for brittle deformation and ductile deformation (shown in grey) are identified. To highlight the changes of deformation modes and the corresponding effect on σ_p, in

the map, the triangles represent the simulated samples for which the deformation is characterized by highly localized shear banding, i.e., brittle deformation, while the stars and circles indicate those showing necking behaviour and homogeneous-like plastic flow, respectively, both of which are manifestations of ductile deformation [12, 75]. The normalized peak stresses (σ_p/σ_{cr}) are also presented and coloured according to the colour scale given in **Fig. 9**, in which a value of 1.0 corresponds to the critical boundary for the transition.

The deformation map demonstrates a clear structural state-dependent critical boundary for the brittle-to-ductile transition in G-MGs. Several apparent features can be observed. Firstly, at low volume fraction and low degree of structural disordering of GRASs in G-MGs, the deformation mode is characterized by highly localized shear banding, similar to the M-MG. While, with increasing the volume fraction and degree of structural disordering across the transition boundary, the deformation mode shifts to ductile necking, and then to homogeneous-like plastic flow. It can be speculated that necking, as an intermediate mode, is mainly concentrated within a narrow regime near the upper side of the transition boundary. Based on this speculation, a boundary for the transition from necking to homogeneous-like plastic flow (N-H) can be roughly drawn in **Fig. 9**, though its location cannot be quantificationally ascertained. Accordingly, an intermediate region between the two transition boundaries, in which the deformation is governed by ductile necking, is identified. It is noted that σ_p/σ_{cr} decreases progressively from the brittle to the ductile regime. Therefore, a good combination of ductility and high strength can to be obtained by tailoring the structural state of G-MGs in this region. Secondly, it is observed that for G-MGs that have a high volume or full occupation of GRASs, the transition appears to be less sensitive to the degree of structural disordering. More specifically, an entirely rejuvenated G-MG is inclined to sustain large plastic deformability, even if the degree of structural disordering is relatively low.

Thirdly and most importantly, there exists a critical value (around 45.7%) for the volume fraction, below which brittle-to-ductile transition would not occur even if the amorphous structures of GRASs in G-MGs are completely rejuvenated. From these results, one can recognize the significance of tailoring a good combination of the volume fraction and degree of structural disordering of GRASs in controlling the overall mechanical properties of G-MGs.

4.5. The effect of aspect ratio on the brittle-to-ductile transition

Before concluding, it is instructive to investigate the effect of aspect ratio (R) on the brittle-to-ductile transition in the partially rejuvenated G-MGs, since samples with large aspect ratios are more meaningful for mechanical tensile tests [20, 23]. The aspect ratios of the above-investigated samples were all fixed to a relatively low value of 2 in order to accommodate a reasonable computational efficiency. It is noteworthy that MGs and MG composites with large aspect ratios tend to exhibit more localized plastic deformation [31, 62]. In the literature, several works [62, 70, 76] associated with stretching small-sized MGs also revealed that samples with high aspect ratios displayed brittle-like deformation behaviour and negligible tensile ductility, whereas those with low aspect ratios demonstrated improved plastic deformability. To examine whether the aspect ratio also influences the transition in the G-MGs, three P60 E4-state G-MGs with different aspect ratios of 2, 4 and 6 (see $\varepsilon = 0$ in **Fig. 10(a)**) were fabricated and the deformation behaviour under tensile loading was examined. For simplicity, the G-MGs are thereafter denoted as $R2$, $R4$ and $R8$, respectively. It should be noted that the P60 E4-state G-MG fabricated with an aspect ratio of 2 displays homogeneous-like plastic deformation behaviour, as revealed in **Fig. 5(c)**. While, as the aspect ratio increases from 2 to 6, a transition of the deformation mode from homogeneous-like plastic flow to necking-like deformation can be clearly identified from **Fig. 10**. This suggests that a large aspect ratio impedes the brittle-to-ductile transition in the irradiation-rejuvenated G-MGs.

Generally, the larger the aspect ratio adopted, the larger the elastic energy release for more unstable shear localization after yielding [77]. Following this viewpoint, one can speculate that the tensile ductility of the partially rejuvenated G-MGs could be further deteriorated with less favourable aspect ratios.

5. Conclusions

The tensile deformation behaviour of $Cu_{64}Zr_{36}$ G-MGs that were partially rejuvenated with different GRASs was systematically investigated by tailoring their volume fraction and degree of structural disordering using atomistic simulations. Valuable insights were gained into understanding the atomistic mechanism of tunable tensile ductility in these partially rejuvenated G-MGs and attempts were also made to identify the critical structural conditions of GRASs required for switching the brittle-to-ductile transition. It was found that the tensile ductility of the G-MGs can be effectively tuned by tailoring the volume fraction and degree of structural disordering of GRASs, although at the expense of some strength. Above critical combinations of the volume fraction and degree of structural disordering of GRASs, the brittle-to-ductile transition can be observed in the G-MGs. The introduced ductile GRASs were found to serve as heterogeneous barriers, suppressing the unstable propagation of shear bands across the GRASs, which in turn promotes the formation and propagation of new shear bands in the unrejuvenated regions. The interactions between the ductile GRASs and the shear bands generated in the unrejuvenated regions contribute to the observed ductility enhancement in the G-MGs. Moreover, the observed structural state-dependent transition of the deformation mode was understood from a mechanical perspective by considering the competition between the macroscopic yield stress and the critical stress required for shear delocalization, and a criterion was introduced to predict the critical transition boundary in G-MGs with GRASs across a wide range of structural states. In

addition, it was found that reducing the sample size promotes the brittle-to-ductile transition in G-MGs, while increasing the aspect ratio impedes the transition. The obtained results not only provide a deep understanding of the structure-property relationship in irradiation-rejuvenated MGs, but also offer significant insights for designing and processing MGs with excellent mechanical properties.

Acknowledgements

This research was fully funded by the Research Committee of the Hong Kong Polytechnic University under research student project account code *RTLR*.

Supplementary data

Supplementary data associated with this article can be found, in the online version at…

References

[1] W.H. Wang, C. Dong, C.H. Shek, Bulk metallic glasses, Mater. Sci. Eng., R 44(2-3) (2004) 45-90.

[2] J. Schroers, Q. Pham, A. Peker, N. Paton, R.V. Curtis, Blow molding of bulk metallic glass, Scripta Mater. 57(4) (2007) 341-344.

[3] M.W. Chen, Mechanical behavior of metallic glasses: Microscopic understanding of strength and ductility, Annu. Rev. Mater. Res. 38 (2008) 445-469.

[4] H. Bei, S. Xie, E.P. George, Softening caused by profuse shear banding in a bulk metallic glass, Phys. Rev. Lett. 96(10) (2006) 105503.

[5] S.H. Chen, K.C. Chan, L. Xia, Deformation behavior of a Zr-based bulk metallic glass under a complex stress state, Intermetallics 43 (2013) 38-44.

[6] A.L. Greer, Y.Q. Cheng, E. Ma, Shear bands in metallic glasses, Mater. Sci. Eng., R 74(4) (2013) 71-132.

[7] J. Lewandowski, W. Wang, A. Greer, Intrinsic plasticity or brittleness of metallic glasses, Philos. Mag. Lett. 85(2) (2005) 77-87.

[8] H.F. Zhou, C. Zhong, Q.P. Cao, S.X. Qu, X.D. Wang, W. Yang, J.Z. Jiang, Non-localized deformation in metallic alloys with amorphous structure, Acta Mater. 68 (2014) 32-41.

[9] S. Pauly, G. Liu, G. Wang, U. Kühn, N. Mattern, J. Eckert, Microstructural heterogeneities governing the deformation of Cu47.5Zr47.5Al5 bulk metallic glass composites, Acta Mater. 57(18) (2009) 5445-5453.

[10] E. Ma, J. Ding, Tailoring structural inhomogeneities in metallic glasses to enable tensile ductility at room temperature, Mater. Today 19(10) (2016) 568-579.

[11] D.H. Kim, W.T. Kim, E.S. Park, N. Mattern, J. Eckert, Phase separation in metallic glasses, Prog. Mater Sci. 58(8) (2013) 1103-1172.
[12] S. Adibi, Z.D. Sha, P.S. Branicio, S.P. Joshi, Z.S. Liu, Y.W. Zhang, A transition from localized shear banding to homogeneous superplastic flow in nanoglass, Appl. Phys. Lett. 103(21) (2013) 211905.
[13] X.L. Wang, F. Jiang, H. Hahn, J. Li, H. Gleiter, J. Sun, J.X. Fang, Plasticity of a scandium-based nanoglass, Scripta Mater. 98 (2015) 40-43.
[14] D. Şopu, K. Albe, Y. Ritter, H. Gleiter, From nanoglasses to bulk massive glasses, Appl. Phys. Lett. 94(19) (2009) 191911.
[15] F. Wu, J. Wei, K. Chan, S. Chen, R. Zhao, G. Zhang, X. Wu, Revealing homogeneous plastic deformation in dendrite-reinforced Ti-based metallic glass composites under tension, Sci. Rep. 7 (2017) 42598.
[16] D.C. Hofmann, J.Y. Suh, A. Wiest, G. Duan, M.L. Lind, M.D. Demetriou, W.L. Johnson, Designing metallic glass matrix composites with high toughness and tensile ductility, Nature 451(7182) (2008) 1085-1089.
[17] Y. Wang, J. Li, A.V. Hamza, T.W. Barbee, Ductile crystalline-amorphous nanolaminates, Prov. Natl. Acad. Sci. 104(27) (2007) 11155-11160.
[18] Q. Wang, Y. Yang, H. Jiang, C.T. Liu, H.H. Ruan, J. Lu, Superior tensile ductility in bulk metallic glass with gradient amorphous structure, Sci. Rep. 4 (2014) 4757.
[19] Y. Zhang, W.H. Wang, A.L. Greer, Making metallic glasses plastic by control of residual stress, Nat. Mater. 5(11) (2006) 857-860.
[20] D.J. Magagnosc, G. Kumar, J. Schroers, P. Felfer, J.M. Cairney, D.S. Gianola, Effect of ion irradiation on tensile ductility, strength and fictive temperature in metallic glass nanowires, Acta Mater. 74 (2014) 165-182.
[21] A.G. Perez-Bergquist, H. Bei, K.J. Leonard, Y. Zhang, S.J. Zinkle, Effects of ion irradiation on Zr52.5Cu17.9Ni 14.6Al10Ti5 (BAM-11) bulk metallic glass, Intermetallics 53 (2014) 62-66.
[22] D.J. Magagnosc, R. Ehrbar, G. Kumar, M.R. He, J. Schroers, D.S. Gianola, Tunable tensile ductility in metallic glasses, Sci. Rep. 3 (2013) 1096.
[23] X.L. Bian, G. Wang, H.C. Chen, L. Yan, J.G. Wang, Q. Wang, P.F. Hu, J.L. Ren, K.C. Chan, N. Zheng, A. Teresiak, Y.L. Gao, Q.J. Zhai, J. Eckert, J. Beadsworth, K.A. Dahmen, P.K. Liaw, Manipulation of free volumes in a metallic glass through Xe-ion irradiation, Acta Mater. 106 (2016) 66-77.
[24] Q. Xiao, L. Huang, Y. Shi, Suppression of shear banding in amorphous ZrCuAl nanopillars by irradiation, J. Appl. Phys. 113(8) (2013) 083514.
[25] S.G. Mayr, Impact of ion irradiation on the thermal, structural, and mechanical properties of metallic glasses, Phys. Rev. B 71(14) (2005) 144109.
[26] K.A. Avchaciov, Y. Ritter, F. Djurabekova, K. Nordlund, K. Albe, Controlled softening of Cu64Zr36 metallic glass by ion irradiation, Appl. Phys. Lett. 102(18) (2013) 181910.
[27] T. Nagase, Y. Umakoshi, Electron irradiation induced crystallization of the amorphous phase in Zr-Cu based metallic glasses with various thermal stability, Mater. Trans. 45(1) (2004) 13-23.
[28] R. Raghavan, K. Boopathy, R. Ghisleni, M.A. Pouchon, U. Ramamurty, J. Michler, Ion irradiation enhances the mechanical performance of metallic glasses, Scripta Mater. 62(7) (2010) 462-465.

[29] Y.H. Liu, F. Zhao, Y.L. Li, M.W. Chen, Deformation behavior of metallic glass thin films, J. Appl. Phys. 112(6) (2012) 063504.
[30] L. Tian, Y.Q. Cheng, Z.W. Shan, J. Li, C.C. Wang, X.D. Han, J. Sun, E. Ma, Approaching the ideal elastic limit of metallic glasses, Nat. Commun. 3 (2012) 609.
[31] D. Şopu, K. Albe, J. Eckert, Metallic glass nanolaminates with shape memory alloys, Acta Mater. 159 (2018) 344-351.
[32] D. Şopu, M. Stoica, J. Eckert, Deformation behavior of metallic glass composites reinforced with shape memory nanowires studied via molecular dynamics simulations, Appl. Phys. Lett. 106(21) (2015) 211902.
[33] L. Zhao, K.C. Chan, S.H. Chen, Atomistic deformation mechanisms of amorphous/polycrystalline metallic nanolaminates, Intermetallics 95 (2018) 102-109.
[34] D. Sopu, A. Stukowski, M. Stoica, S. Scudino, Atomic-level processes of shear band nucleation in metallic glasses, Phys. Rev. Lett. 119(19) (2017) 195503.
[35] S. Plimpton, Fast parallel algorithms for short-range molecular dynamics, J. Comput. Phys. 117(1) (1995) 1-19.
[36] Y.S. Yun, B.J. Kim, J.H. Na, H.S. Nam, P.R. Cha, W.T. Kim, D.H. Kim, The effect of enthalpy of mixing on the atomic level structure and plasticity of amorphous alloys: A molecular dynamics simulation study in a binary model system, Intermetallics 92 (2018) 25-35.
[37] S.D. Feng, L. Qi, L.M. Wang, S.P. Pan, M.Z. Ma, X.Y. Zhang, G. Li, R.P. Liu, Atomic structure of shear bands in Cu64Zr36 metallic glasses studied by molecular dynamics simulations, Acta Mater. 95 (2015) 236-243.
[38] Y.Q. Cheng, E. Ma, H.W. Sheng, Atomic level structure in multicomponent bulk metallic glass, Phys. Rev. Lett. 102(24) (2009) 245501.
[39] F. Shimizu, S. Ogata, J. Li, Theory of shear banding in metallic glasses and molecular dynamics calculations, Mater. Trans. 48(11) (2007) 2923-2927.
[40] Z.D. Sha, P.S. Branicio, H.P. Lee, T.E. Tay, Strong and ductile nanolaminate composites combining metallic glasses and nanoglasses, Int. J. Plast. 90 (2017) 231-241.
[41] Y.Q. Cheng, A.J. Cao, E. Ma, Correlation between the elastic modulus and the intrinsic plastic behavior of metallic glasses: The roles of atomic configuration and alloy composition, Acta Mater. 57(11) (2009) 3253-3267.
[42] A. Stukowski, Visualization and analysis of atomistic simulation data with OVITO-the Open Visualization Tool, Modell. Simul. Mater. Sci. Eng. 18(1) (2009) 015012.
[43] G. Duan, D. Xu, Q. Zhang, G. Zhang, T. Cagin, W.L. Johnson, W.A. Goddard Iii, Molecular dynamics study of the binary Cu46Zr54 metallic glass motivated by experiments: Glass formation and atomic-level structure, Phy. Rev. B 71(22) (2005) 224208.
[44] S.P. Pan, J.Y. Qin, W.M. Wang, T.K. Gu, Origin of splitting of the second peak in the pair-distribution function for metallic glasses, Phy. Rev. B 84(9) (2011) 092201.
[45] J. Ding, E. Ma, M. Asta, R.O. Ritchie, Second-nearest-neighbor correlations from connection of atomic packing motifs in metallic glasses and liquids, Sci. Rep. 5 (2015) 17429.
[46] A.J. Cao, Y.Q. Cheng, E. Ma, Structural processes that initiate shear localization in metallic glass, Acta Mater. 57(17) (2009) 5146-5155.

[47] K.H. Kang, K.W. Park, J.C. Lee, E. Fleury, B.J. Lee, Correlation between plasticity and other materials properties of Cu-Zr bulk metallic glasses: An atomistic simulation study, Acta Mater. 59(2) (2011) 805-811.
[48] M. Wakeda, Y. Shibutani, Icosahedral clustering with medium-range order and local elastic properties of amorphous metals, Acta Mater. 58(11) (2010) 3963-3969.
[49] Q.K. Li, M. Li, Free volume evolution in metallic glasses subjected to mechanical deformation, Mater. Trans. 48(7) (2007) 1816-1821.
[50] J. Heo, S. Kim, S. Ryu, D. Jang, Delocalized plastic flow in proton-irradiated monolithic metallic glasses, Sci. Rep. 6 (2016) 23244.
[51] Q. Zhang, Q.K. Li, M. Li, Key factors affecting mechanical behavior of metallic glass nanowires, Sci. Rep. 7 (2017) 41365.
[52] Q. Zhang, Q.K. Li, M. Li, Internal stress and its effect on mechanical strength of metallic glass nanowires, Acta Mater. 91 (2015) 174-182.
[53] D. Sopu, C. Soyarslan, B. Sarac, S. Bargmann, M. Stoica, J. Eckert, Structure-property relationships in nanoporous metallic glasses, Acta Mater. 106 (2016) 199-207.
[54] C. Zhong, H. Zhang, Q.P. Cao, X.D. Wang, D.X. Zhang, U. Ramamurty, J.Z. Jiang, Deformation behavior of metallic glasses with shear band like atomic structure: A molecular dynamics study, Sci. Rep. 6 (2016) 30935.
[55] D. Șopu, Y. Ritter, H. Gleiter, K. Albe, Deformation behavior of bulk and nanostructured metallic glasses studied via molecular dynamics simulations, Phy. Rev. B 83(10) (2011) 100202.
[56] Z.D. Sha, S.X. Qu, Z.S. Liu, T.J. Wang, H. Gao, Cyclic Deformation in Metallic Glasses, Nano Lett. 15(10) (2015) 7010-7015.
[57] S. Adibi, P.S. Branicio, S.P. Joshi, Suppression of shear banding and transition to necking and homogeneous flow in nanoglass nanopillars, Sci. Rep. 5 (2015) 15611.
[58] D. Jang, J.R. Greer, Transition from a strong-yet-brittle to astronger-and-ductile state by size reductionofmetallicglasses, Nat. Mater. 9(3) (2010) 215-219.
[59] H. Guo, P.F. Yan, Y.B. Wang, J. Tan, Z.F. Zhang, M.L. Sui, E. Ma, Tensile ductility and necking of metallic glass, Nat. Mater. 6(10) (2007) 735-739.
[60] C. Zhong, H. Zhang, Q.P. Cao, X.D. Wang, D.X. Zhang, J.W. Hu, P.K. Liaw, J.Z. Jiang, Non-localized deformation in Cu-Zr multi-layer amorphous films under tension, J. Alloys Compd. 678 (2016) 410-420.
[61] D.Z. Chen, D. Jang, K.M. Guan, Q. An, W.A. Goddard, J.R. Greer, Nanometallic glasses: Size reduction brings ductility, surface state drives its extent, Nano Lett. 13(9) (2013) 4462-4468.
[62] D. Șopu, A. Foroughi, M. Stoica, J. Eckert, Brittle-to-ductile transition in metallic glass nanowires, Nano Lett. 16(7) (2016) 4467-4471.
[63] C. Zhong, H. Zhang, Q.P. Cao, X.D. Wang, D.X. Zhang, U. Ramamurty, J.Z. Jiang, On the critical thickness for non-localized to localized plastic flow transition in metallic glasses: A molecular dynamics study, Scripta Mater. 114 (2016) 93-97.
[64] C. Zhong, H. Zhang, Q.P. Cao, X.D. Wang, D.X. Zhang, J.Z. Jiang, The size-dependent non-localized deformation in a metallic alloy, Scripta Mater. 101 (2015) 48-51.

[65] Y.F. Shi, Size-independent shear band formation in amorphous nanowires made from simulated casting, Appl. Phys. Lett. 96(12) (2010) 121909.
[66] Q.K. Li, M. Li, Atomic scale characterization of shear bands in an amorphous metal, Appl. Phys. Lett. 88(24) (2006) 241903.
[67] S. Scudino, J.J. Bian, H.S. Shahabi, D. Sopu, J. Sort, J. Eckert, G. Liu, Ductile bulk metallic glass by controlling structural heterogeneities, Sci. Rep. 8 (2018) 9174.
[68] B. Arman, C. Brandl, S. Luo, T. Germann, A. Misra, T. Çağin, Plasticity in Cu (111)/Cu46Zr54 glass nanolaminates under uniaxial compression, J. Appl. Phys. 110(4) (2011) 043539.
[69] B. Cheng, J.R. Trelewicz, Mechanistic coupling of dislocation and shear transformation zone plasticity in crystalline-amorphous nanolaminates, Acta Mater. 117 (2016) 293-305.
[70] Z.D. Sha, L.C. He, Q.X. Pei, Z.S. Liu, Y.W. Zhang, T.J. Wang, The mechanical properties of a nanoglass/metallic glass/nanoglass sandwich structure, Scripta Mater. 83 (2014) 37-40.
[71] D. Şopu, K. Albe, Influence of grain size and composition, topology and excess free volume on the deformation behavior of Cu-Zr nanoglasses, Beilstein J. Nanotech. 6(1) (2015) 537-545.
[72] C.A. Volkert, A. Donohue, F. Spaepen, Effect of sample size on deformation in amorphous metals, J. Appl. Phys. 103(8) (2008) 083539.
[73] C.Q. Chen, Y.T. Pei, J.T.M. De Hosson, Effects of size on the mechanical response of metallic glasses investigated through in situ TEM bending and compression experiments, Acta Mater. 58(1) (2010) 189-200.
[74] R.D. Conner, R.B. Dandliker, W.L. Johnson, Mechanical properties of tungsten and steel fiber reinforced Zr41.25Ti13.75Cu12.5Ni10Be22.5 metallic glass matrix composites, Acta Mater. 46(17) (1998) 6089-6102.
[75] S. Adibi, P.S. Branicio, Y.W. Zhang, S.P. Joshi, Composition and grain size effects on the structural and mechanical properties of CuZr nanoglasses, J. Appl. Phys. 116(4) (2014) 043522.
[76] J. Yi, W.H. Wang, J.J. Lewandowski, Sample size and preparation effects on the tensile ductility of Pd-based metallic glass nanowires, Acta Mater. 87 (2015) 1-7.
[77] Z.D. Sha, L.C. He, S. Xu, Q.X. Pei, Z.S. Liu, Y.W. Zhang, T.J. Wang, Effect of aspect ratio on the mechanical properties of metallic glasses, Scripta Mater. 93 (2014) 36-39.

Figure captions

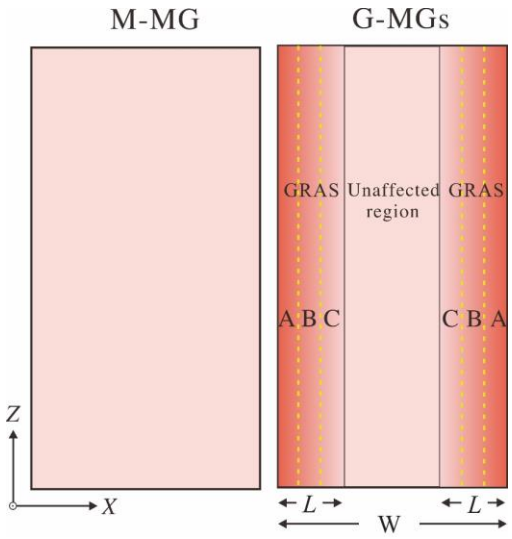

Fig. 1. The schematic illustrations of the M-MG and G-MGs, demonstrating the distribution of GRASs.

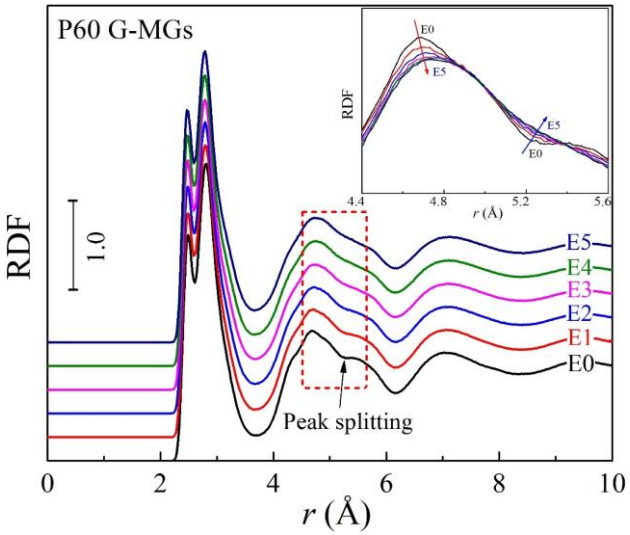

Fig. 2. The calculated RDFs for the P60 G-MGs prepared by different times of atomic rearrangement. **Inset:** The enlarged patterns around the second maxima as marked by the red box, which reveals a structural disordering process.

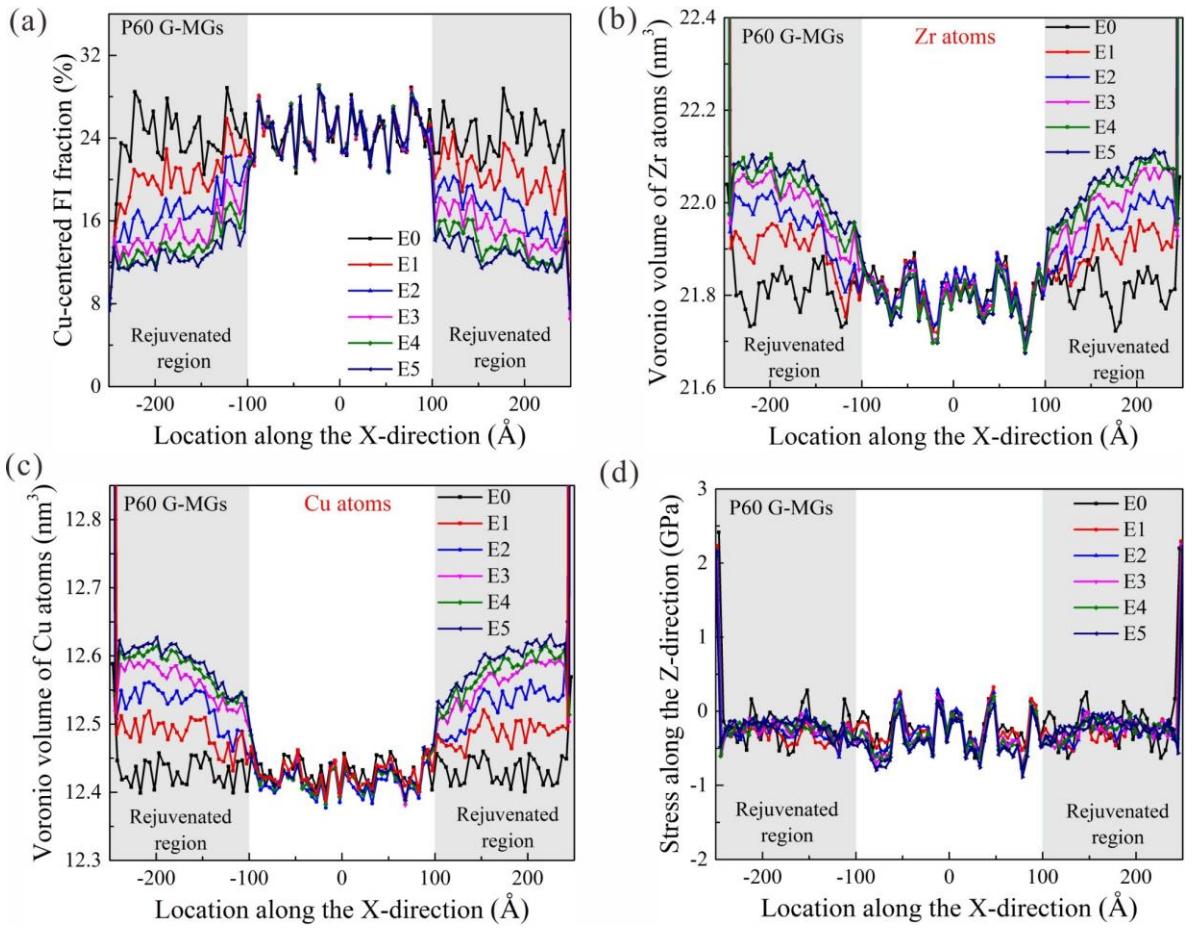

Fig. 3. Several selected parameters revealing the GRASs in the 50 nm-wide P60 G-MGs prepared after different times of atomic rearrangements. **(a)** The evolution of the Cu-centered FI fractions; **(b)** The variations of the local atomic Voronoi volume of Zr type atoms and **(c)** Cu type atoms; **(d)** The profiles of local average stress along the Z-direction. The values of the horizontal axis refer to the location with respect to the center of the samples along the X-direction; the bin size for sampling is 5.0 Å.

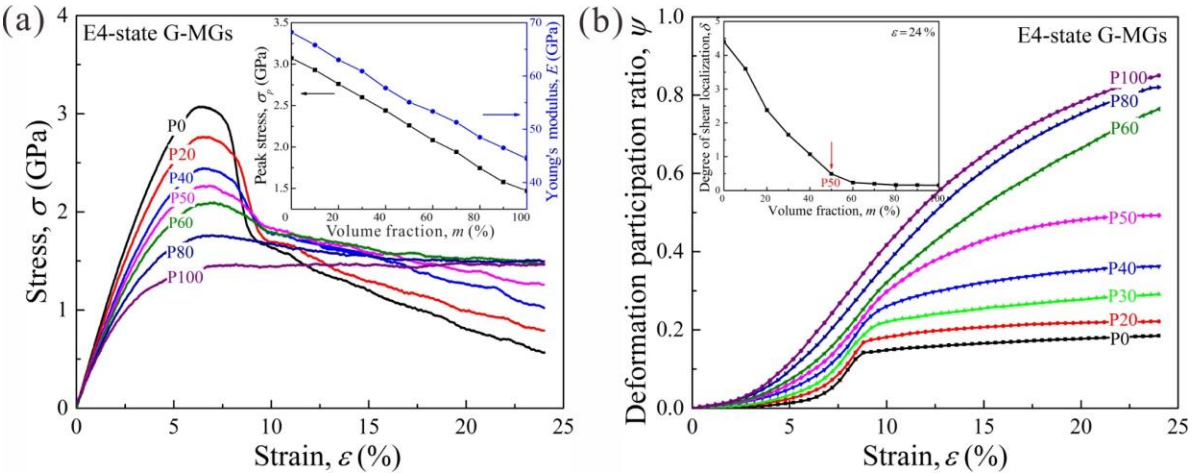

Fig. 4. (a) Representative tensile SS of the E4-state G-MGs prepared with different volume fractions of GRASs. **Inset:** The evolution of Young's modulus (E) and the peak stress (σ_p) as a function of volume fraction. **(b)** The evolution of ψ as a function of the applied strain. **Inset:** The evolution of δ as a function of volume fraction at ε = 24%. The arrow highlights the critical volume fraction of GRASs required for the transition.

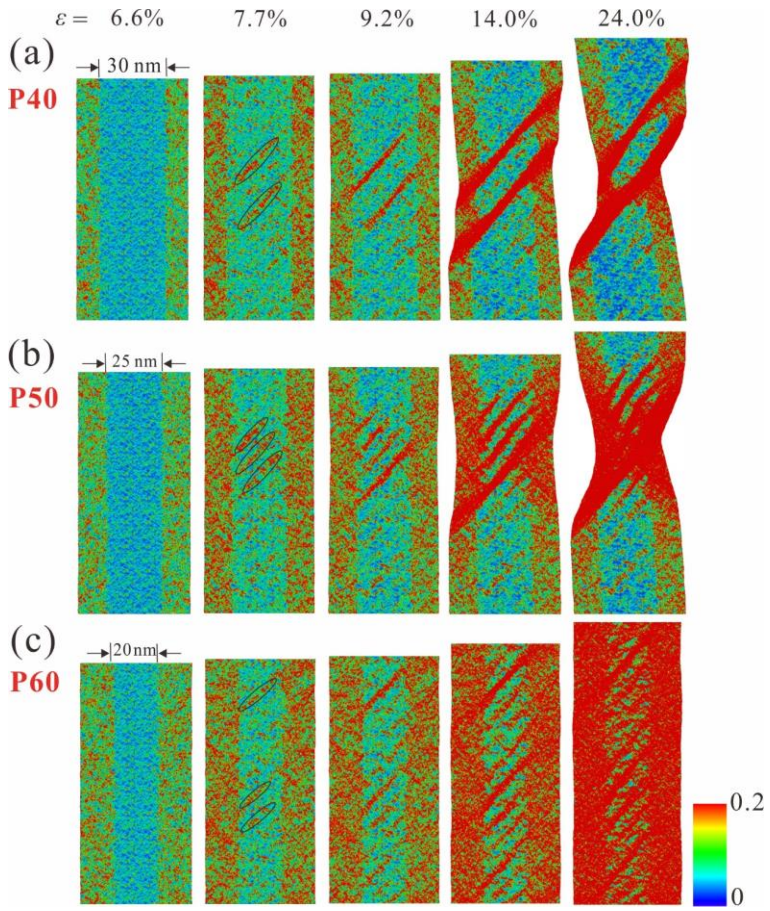

Fig. 5. Deformation snapshots of η^{Mises} for **(a)** the P40, **(b)** P50 and **(c)** P60 E4-state G-MGs under different applied strains, demonstrating a transition of the deformation mode around the critical volume fraction of 50%. The nucleation sites of the initial generated embryonic shear bands are marked by the ellipses. To identify the nucleation sites, the inspection interval of the deformation process was chosen as low as 0.1%. In simulations, the shear bands were stochastically generated in different samples along two equivalent directions, i.e., approximately along the maximum shear plane. For comparison, they were adjusted to the same direction in all the samples.

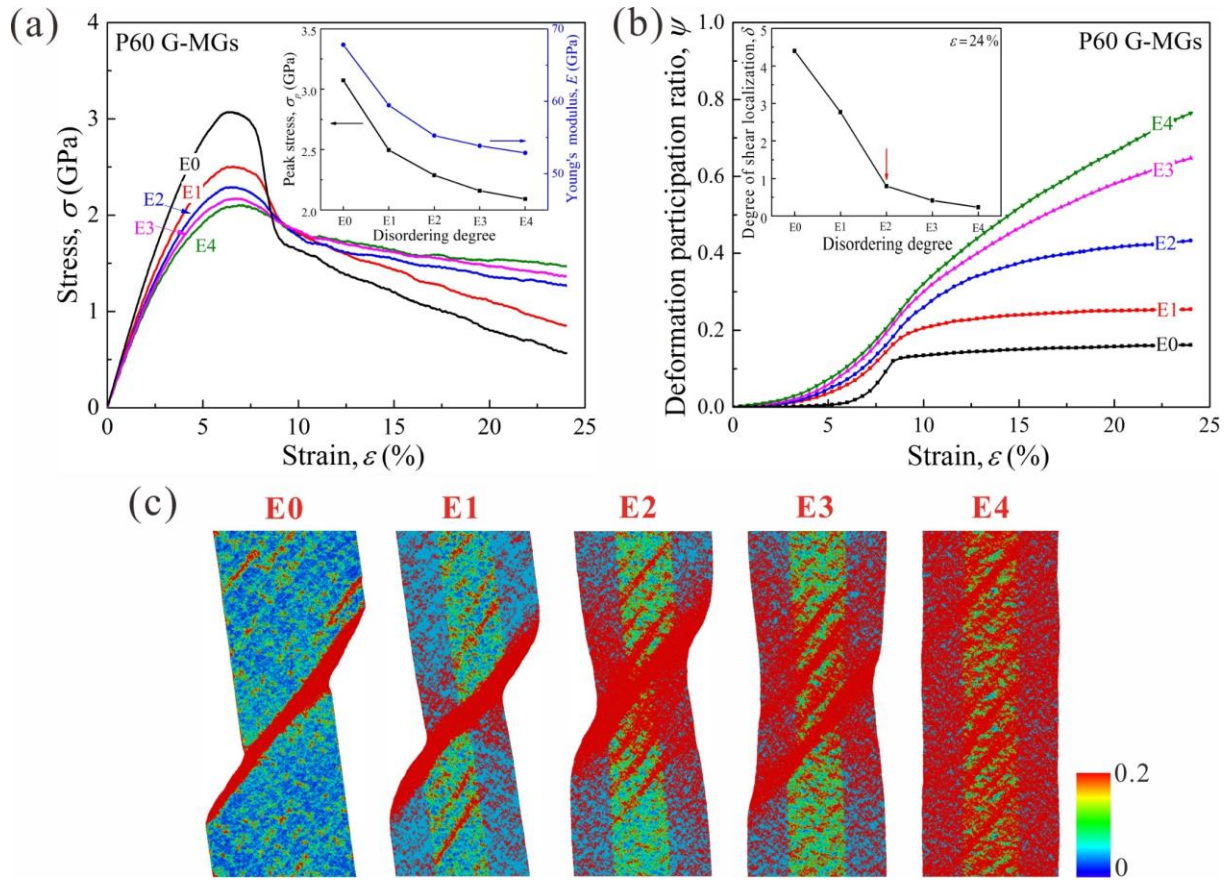

Fig. 6. Effect of degree of structural disordering of GRASs on the tensile deformation behaviour of the P60 G-MGs. **(a)** The tensile SS curves. **Inset:** The evolution of σ_p and E as a function of the degree of structural disordering. **(b)** The evolution of ψ as a function of the applied strain. **Inset:** The evolution of δ as a function of the degree of structural disordering at ε = 24%. The arrow highlights the critical degree of structural disordering of GRASs required for the transition. **(c)** The deformation patterns of the P60 G-MGs at ε = 24%, revealing the transition of the deformation mode.

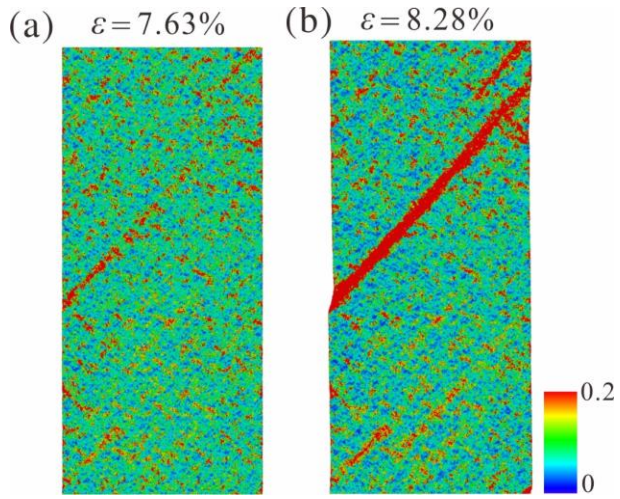

Fig. 7. Deformation snapshots of the M-MG upon shear banding: **(a)** The critical point for shear band initiation on the left surface at ε = 7.63%. **(b)** The critical point for the shear band penetrating the entire sample at ε = 8.28%.

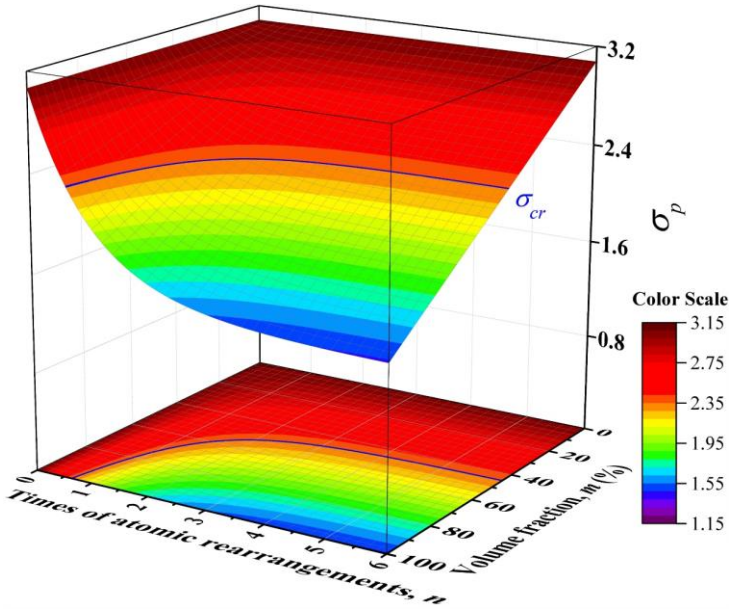

Fig. 8. The evolution of σ_p in the G-MGs with GRASs across a wide range of structural states, as predicted by the parameterized σ_p.

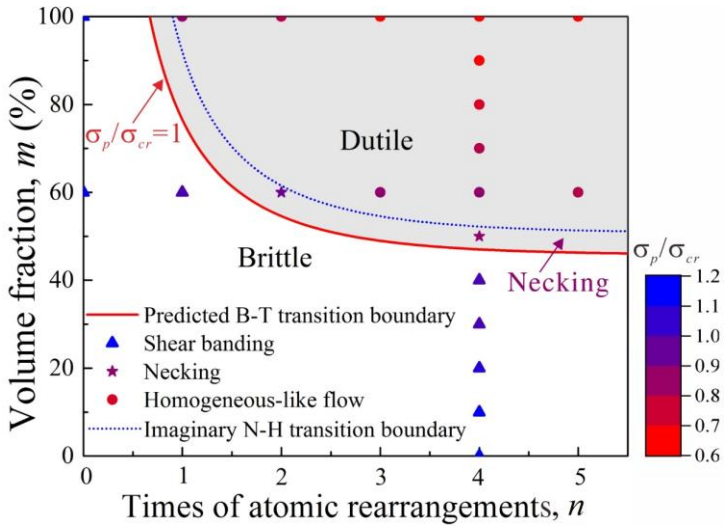

Fig. 9. The deformation map illustrating the influence of degree of structural disordering and volume fraction of GRASs on the critical transition boundary between brittle and ductile deformation. The solid line is the predicated transition boundary drawn according to the criterion for non-localized deformation. To facilitate identifying different deformation modes, the normalized peak stresses (σ_p/σ_{cr}) of the simulated samples are also presented and coloured according to the given colour scale.

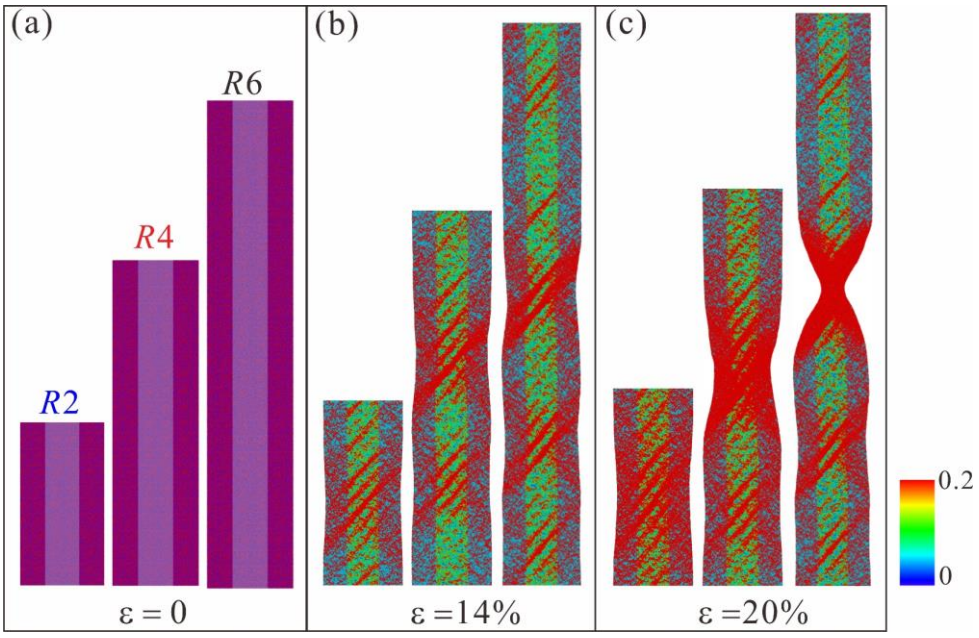

Fig. 10. Deformation snapshots of η^{Mises} for the series of the P60 E4-state G-MGs fabricated with different aspect ratios under the applied strains of **(a)** $\varepsilon = 0$, **(b)** $\varepsilon = 14\%$ and **(c)** $\varepsilon = 20\%$, respectively.

Supplementary Materials

Tunable tensile ductility of metallic glasses with partially rejuvenated amorphous structures

L. Zhao [a], K.C. Chan [a,*], S.H. Chen [b], S.D. Feng [a], D.X. Han [a], G. Wang [c]

[a] *Advanced Manufacturing Technology Research Centre, Department of Industrial and Systems Engineering, The Hong Kong Polytechnic University, Hung Hom, Kowloon, Hong Kong*

[b] *School of Mechanical Engineering, Hefei University of Technology, Hefei 230009, China*

[c] *Laboratory for Microstructures, Institute of Materials, Shanghai University, Shanghai 200444, China*

I. The effect of degree of structural disordering of GRASs on the tensile deformation behaviour

To examine the effect of degree of structural disordering of GRASs on the tensile deformation behaviour in G-MGs, a sequence of deformation patterns under different applied strains in the P60 G-MGs fabricated with different degrees of structural disordering of GRASs were supplemented in **Fig. S1**. The deformation process was examined with a strain interval as low as 0.1% to identify the nucleation sites of shear bands in the samples (see ε =7.7% in **Fig. S1**).

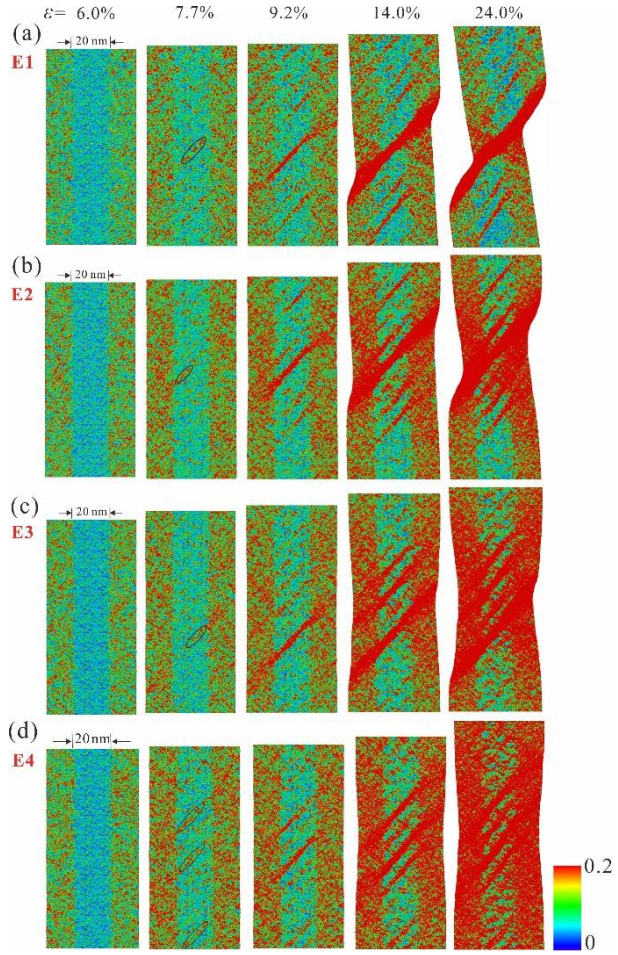

Fig. S1. Deformation snapshots of η^{Mises} for the **(a)** E1, **(b)** E2, **(c)** E3 and **(d)** E4-state P60 G-MGs under different applied strains, demonstrating a transition of the deformation mode around the critical degree of structural disordering of the E2-state. The nucleation sites of the initial generated embryonic shear bands are marked by the ellipses.

II. The effect of sample size on the brittle-to-ductile transition

To examine the effect of sample size on the brittle-to-ductile transition, the sample width (W) was reduced from 50 nm to 30 nm, while the aspect ratio of the samples is fixed to 2. For simplicity, the G-MGs prepared with different sample widths were thereafter denoted as Wl, where l is the sample width (i.e., 50 and 30, respectively). The same tensile deformation condition (see **Simulation Methods**) was applied on the W30 E4-state G-MGs. The tensile deformation behaviour of two series of E4-state G-MGs prepared with different volume fractions of GRASs were examined. **Fig. S2(a)** shows that a striking increase of ψ (see **Simulation Methods**) is observed as the volume fraction of GRASs crosses 40%, which corresponds to the critical condition required for the transition in the W30 E4-state G-MGs. The evolution of δ (see **Simulation Methods**) as a function of the volume fraction at ε = 24%, as shown **Fig. S2(b)**, demonstrates that δ shifts to lower values as W decreases from 50 nm to 30 nm. This indicates that small sample size tends to promote more homogenous plastic deformation in G-MGs that were prepared with the same structural state. The deformation patterns of the W30 E4-state G-MGs at ε = 24%, as shown **Fig. S2(c)**, evidently demonstrate a transition of the deformation mode around the critical volume fraction of 40%. As illuminated in **Section 3.2**, in the W50 E4-state G-MGs the transition takes places as the volume fraction of GRASs reaches 50% (**Fig.5(b)**). From the above analysis, one can recognize that reducing the sample size promotes the brittle-to-ductile transition in G-MGs.

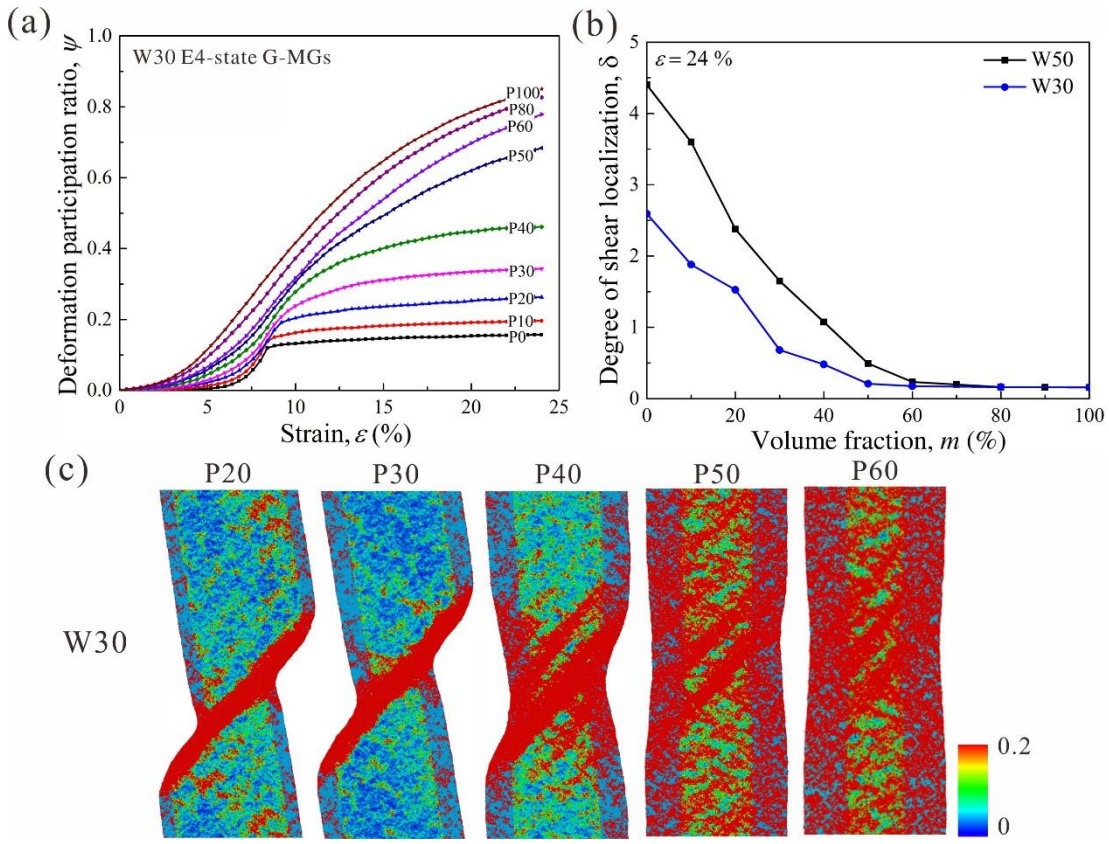

Fig. S2. Effect of sample size on the brittle-to-ductile transition in the E4-state G-MGs. **(a)** The evolution of ψ as a function of the applied strain in the W30 E4-state G-MGs. **(b)** The evolution of δ as a function of volume fraction at ε = 24%. **(c)** The deformation patterns of the W30 E4-state G-MGs at ε = 24%, revealing a transition of the deformation mode around the critical volume fraction of 40%.

III. Prediction of σ_p in G-MGs with GRASs across a wide range of structural states

It was demonstrated that increasing both the volume fraction and the degree of structural disordering of GRASs are beneficial to the ductility improvement of G-MGs. While, σ_p and ductility decreases inversely, which are detrimental to the load-bearing capacity of the material. To obtain a sought-after combination of improved ductility and high strength in G-MGs, there needs a trade-off between the ductility and σ_p by controlling the volume fraction and the degree of

structural disordering of GRASs. Therefore, it is instructive to construct a model to predict the evolution of σ_p in G-MGs with GRASs across a wide range of structural states. To this end, the rule of mixtures in iso-strain conditions was introduced. As seen from **Fig. 1**, the G-MGs were constituted with an intact region and two symmetric irradiated regions having different volume fractions and different degrees of structural disordering of GRASs. It is noted that the intact region has the similar structure with the M-MG, as evidenced by the overlapping profiles of the Cu-centred FI friction and the local average Voronoi volumes of the Zr and Cu atoms shown in **Fig. 2**. Meanwhile, it is conceivable that the two separated irradiated regions can be hypothetically combined into a P100 G-MG, which has the same degree of structural disordering of GRASs but with reduced sample size. Therefore, without considering size effect, σ_p of any partially rejuvenated G-MG can be estimated by the rule of mixtures,

$$\sigma_p = \sigma_{M\text{-}MG} \times (100\text{-}m)/100 + \sigma_p(n) \times m/100 \qquad \textbf{(Eq. S1)}$$

where m is the volume fraction of the GRAS in the G-MG, and n is the required times of atomic arrangements for generating the same degree of structural disordering of the GRAS in the corresponding P100 G-MG. $\sigma_{M\text{-}MG}$ is the ultimate tensile strength (3.07 GPa) of the M-MG, i.e., the E0-state G-MG. $\sigma_p(n)$ describes the evolution of the ultimate tensile strength in the P100 G-MGs as a function of the times of atomic rearrangements.

To determine $\sigma_p(n)$ in **Eq. S1**, tensile simulations were further conducted on five P100 G-MGs, which have different degrees of structural disordering of GRASs ranging from the E1 to E5 state. The stress-strain curves are shown in **Fig. S3(a)**, and the extracted σ_p as a function of the degree of structural disordering is plotted in **Fig. S3(b)**. Regardless of the degree of structural disordering of GRASs, all the P100 G-MGs show homogeneous-like deformation behavior due to the entire occupation of the rejuvenated GRASs throughout the samples. Meanwhile, with

increasing the degree of structural disordering of GRASs from the E1 to E5 state, σ_p shows a tendency that first declines and then reaches a plateau (**Fig. S3(b)**). It was found that a power law in the form of $\sigma_p=a+b\times\exp(c\times n)$ can well fit the data, where a, b and c are the fitting parameters; The parameter a in the equation reflects the lower limit of the ultimate tensile strength of the P100 G-MG in an extreme case that the sample is fully rejuvenated. After nonlinear fitting, $\sigma_p(n)$ was determined as follows:

$$\sigma_p(n) = 1.45+1.62\times\exp(-0.911\times n) \quad \text{GPa} \qquad (\textbf{Eq. S2})$$

By incorporating **Eq. S2** into **Eq. S1**, the structural state-dependent σ_p of any given G-MG then can be predicted by specifying the volume fraction and degree of structural disordering of GRASs.

To examine the prediction accuracy, **Eq. S1** was further verified using those σ_p obtained from the simulated G-MGs (see the **inset of Fig. 4(a)** and **inset of Fig. 6(a)**). For clarity, the conditions for the two sets of the simulated G-MGs were considered separately. For the series of the E4-state G-MGs prepared with different volume fractions of GRASs, $\sigma_p=\sigma_{M\text{-}MG}\times(100-m)/100+\sigma_p(n=4)\times m/100$. While for the series of the P60 G-MGs prepared with different degrees of structural disordering of GRASs, $\sigma_p=\sigma_{M\text{-}MG}\times40\%+\sigma_p(n)\times60\%$. The predicted curves in the two conditions are plotted in **Fig. S4(b)** and **Fig. S4(b)**, respectively, together with the corresponding simulated data for comparison. It clear that that the prediction equation, **Eq. S1**, can capture the simulated data of the two sets of G-MGs with reasonable accuracy. From this analysis, we speculate that they may also be capable of describing σ_p of G-MGs with GRASs across a wide range of structural states.

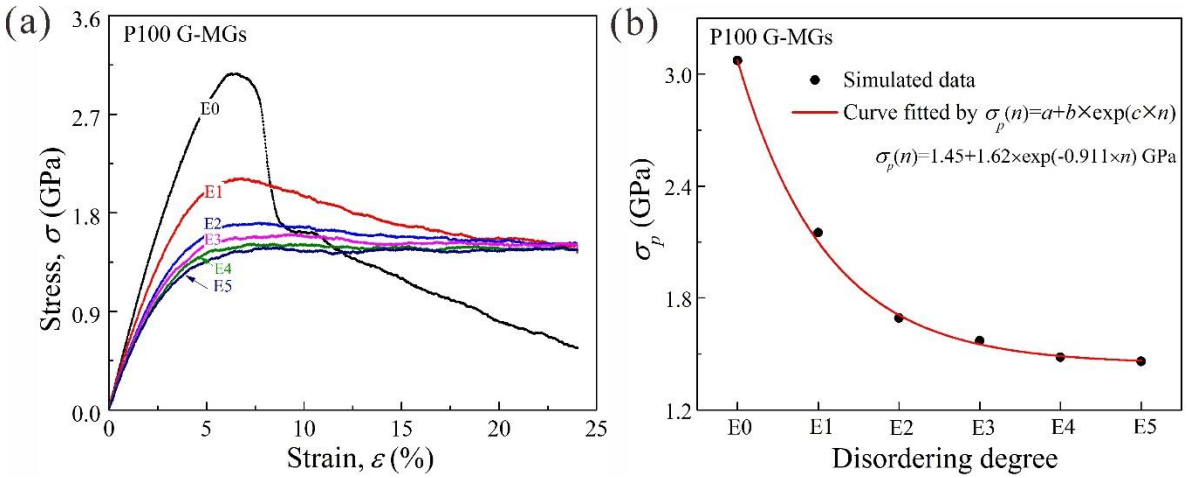

Fig. S3. (a) The stress-strain curves for the P100 G-MGs prepared with different disordering degrees of GRASs ranging from the E0 to E5 state. **(b)** The evolution of σ_p as a function of the disordering degree. The solid circles denote the obtained σ_p from the stress-strain curves, while the line represents the curve fitted by $\sigma_p=a+b\times\exp(c\times n)$.

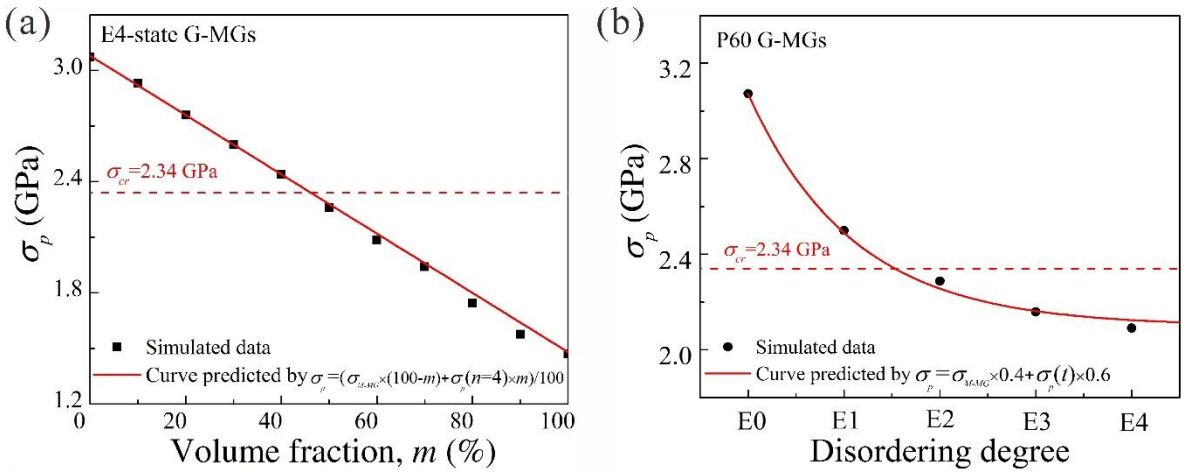

Fig. S4. The comparison between the predicted curves and the data obtained from the simulated samples: **(a)** the E4-state G-MGs prepared with different volume fractions of GRASs; **(b)** the P60 G-MGs prepared with different disordering degrees of GRASs. The solid circles denote the obtained σ_p from the simulated G-MGs, while the lines represent the curves predicted by the model. The dotted lines represent the critical stress (σ_{cr}) for the transition of the deformation mode.